Collision-induced absorption and annihilation in hadronic atoms within a close-coupling approach

V. P. Popov* and V. N. Pomerantsev†

Skobeltsyn Institute of Nuclear Physics, Lomonosov Moscow State University, 119234 Moscow, Russia

(Received 4 July 2012; revised manuscript received 24 September 2012; published 29 November 2012)

The induced absorption or annihilation of π^-, K^-, and $\bar{p}$ in collisions of hadronic hydrogen atoms in excited states with ordinary hydrogen in the ground state is treated in a unified manner with the elastic scattering, Stark transition, and Coulomb de-excitation in the framework of the close-coupling approach. The close-coupling approach is generalized to include both open andclosed channels corresponding to stable and unstable states of the hadronic atom. Calculations are performed using the basis sets including all states of hadronic atoms with a principal quantum number from $n = 1$ up to $n_{\max} = 8$. The general features of induced-absorption cross sections are studied in a wide range of complex energy-shift values. The cross sections of all processes are calculated for $\pi^- p$, $K^- p$, and $\bar{p}p$ atoms with principal quantum numbers $n = 2$–8 and kinetic energies from 0.001 up to 100 eV. The validity of the previous quantum-mechanical and semiclassical models is critically discussed.

DOI: 10.1103/PhysRevA.86.052520 PACS number(s): 36.10.−k

I. INTRODUCTION

The close-coupling approach (CCA) is widely used to describe the collisional processes of composite particles in atomic, molecular, and nuclear physics. In this approach the total wave function of the system is expanded in terms of the basis L_2 functions corresponding to the stationary states of the subsystems. The expansion coefficients are the wave functions of the relative motion of subsystems in open or closed channels. As a result, the multichannel scattering problem is obtained.

However, the excited states of all real quantum-mechanical systems and even some ground states (e.g., hadronic atoms) have finite lifetimes, i.e., are unstable. It is usually assumed that the lifetimes τ of these states are much longer than the collision time $\tau_{\rm coll}$,

$$\tau \gg \tau_{\rm coll} \approx R_0/v, \tag{1}$$

where R_0 denotes the radius of interaction and v is the velocity of relative motion. States satisfying the qualitative condition, Eq. (1), are considered to be stable ones.

In most problems of atomic and nuclear collisions this qualitative condition is fulfilled. However, in our case, when one of the colliding subsystems is a hadronic atom $(X^- a)_{nl}$ ($X^- = \pi^-$, K^-, $\bar{p}$, etc.; $a = p,d,t$ are the hydrogen isotopes; n and l denote the principal and angular momentum quantum numbers, respectively), the stationarity condition, Eq. (1), can be strongly violated in channels corresponding to low angular-momentum states. In addition, it will be noted that this condition makes no sense and cannot be applied in the case of closed channels corresponding to unstable states.

Hadronic hydrogen-like atoms $(X^- a)_{nl}$ are formed in highly excited atomic $(n\,l)$ states after slowing-down and Coulomb capture of negatively charged particles X^- in the hydrogen media. The general features of hadronic hydrogen atoms are similar to those of ordinary hydrogen, since its level structure is mainly formed by static Coulomb interaction. However, in contrast to ordinary hydrogen, the energy levels of low-angular-momentum states of hadronic atoms have a complex energy shift ΔE_{nl} determined by a strong hadron-nucleon interaction. Such states can be called quasidiscrete states, and free hadronic atoms in these states have finite lifetimes τ_{nl} and decay due to nuclear reactions:

$$\pi^- p \longrightarrow \pi^0 n, \gamma n, \tag{2}$$

$$K^- p \longrightarrow \Sigma^{\pm}\pi^{\mp}, \Sigma^0\pi^0, \Lambda n, \tag{3}$$

$$\bar{p}p \longrightarrow \pi^+\pi^-, \pi^0\pi^0, K^+K^-, \pi^0\pi^0\pi^0, \pi^0\omega. \tag{4}$$

The lifetimes of these states $\tau_{nl} = \hbar/\Gamma_{nl}$ are determined by an imaginary part,

$$\Gamma_{nl} = -2\,{\rm Im}\Delta E_{nl}, \tag{5}$$

of the complex energy shift. The width Γ_{nl} determines the nuclear reaction rates from the (nl) state. The problem of taking short-lived states into account is a general one in the stationary scattering theory and should arise in any theoretical approach describing the scattering processes of similar systems (e.g., see [1–9]).

There are at least two mechanisms leading to the decay of hadronic hydrogen-like atoms due to strong-interaction effects. In the first of them the above-mentioned reactions occur from the ns sublevels of hadronic atoms populated in the preceding radiative, Auger, Coulomb, or Stark transitions $nl \to n's$ ($n' \leqslant n$). In the other mechanism, the interaction with the target atom or molecule results in a strong coupling between the stable and the unstable states of hadronic atoms and the absorption or annihilation from the stable states of hadronic atoms takes place during the collision. This process is called *collision-induced absorption* or *annihilation*. The consequences of this mechanism can be observed in both the absolute x-ray yields and the kinetic energy distributions of hadronic atoms at the instant of radiative transitions or nuclear reactions.

According to our knowledge, the effect of nuclear absorption during hadronic hydrogen–ordinary hydrogen collisions has been treated in the framework of the semiclassical straight-line-trajectory approximation [1–4] since the paper by Leon and Bethe [1]. This relatively simple model is only justified if the energy of collision is sufficiently high. A simple

*popov@nucl-th.sinp.msu.ru
†pomeran@nucl-th.sinp.msu.ru

estimation shows that the semiclassical straight-line-trajectory description is valid at collisional energies more than or about several electron volts and therefore a very important range of low-energy collisions cannot be reliably treated.

Noticeable progress in the study of induced absorption in hadronic hydrogen was made by Jensen and Markushin (see [4] and references therein). The quantum close-coupling method was applied by the authors, with the additional assumption that the widths Γ_{ns} are switched off at the interatomic separation $R \geqslant R_g$ (R_g denotes a switched-off parameter used by the authors). However, it is well known that in the potential scattering theory the procedure to switch the interaction on or off is ambiguous and leads, in the general case, to parameter-dependent results. As will be seen below, the cross sections of collision-induced absorption and, especially, the Stark transition very strongly depend on the value of the switched-off parameter used in [4]. In addition, it will be noted that the asymptotic boundary conditions of this model are in contradiction with the ones of the initial scattering problem.

Recently, the problem was considered by Korenman and Yudin [7] in the framework of the CCA by applying the correct asymptotic boundary conditions. The cross sections of the induced annihilation during $(\bar{p}\mathrm{He})^+_{nl} + \mathrm{He}$ collisions for $n = 30$ and $l \geqslant 2$ were calculated in [8] at a fixed energy $E = 10$ K.

However, collision-induced absorption or annihilation in hadronic $(\pi^- p)$, $(K^- p)$, and $(\bar{p}p)$ atoms with the correct asymptotic boundary conditions have not been considered until now. Besides, the effects of the closed channels corresponding to quasidiscrete states were not taken into account in either the close-coupling model [4] or the CCA applied in [7] and [8]. These channels in the case of kaonic and antiprotonic atoms are very important for the realistic description of both elastic scattering and, especially, collision-induced absorption in the wide energy range below $nl - ns$ thresholds ($l \geqslant 1$). The effects of collision-induced absorption on the values of the x-ray yields and kinetic energy distributions of hadronic atoms in lower states are very important in connection with high-precision experiments on the spectroscopy of the lowest levels of $(\pi^- p)$, $(K^- p)$, and $(\bar{p}p)$ atoms. Hence, a more reliable and systematic framework free of *ad hoc* assumptions is necessary to describe this process.

The main motivation of the present paper is to give a consistent quantum-mechanical treatment of hadronic hydrogen–hydrogen atom collisional processes including *ab initio* consideration of the least studied theoretically collision-induced absorption in $(\pi^- p)$ and $(K^- p)$ atoms or annihilation in the case of the $(\bar{p}p)$ atom. Some of our preliminary results obtained in the framework of the CCA were recently published [10].

The paper is organized as follows. Section II is devoted to the unified description of collision-induced absorption together with other collisional processes—Stark mixing, Coulomb de-excitation, and elastic scattering—in the framework of the CCA. In Sec. III the method is applied to study the main regularities of the collision-induced absorption cross sections and to calculate the cross sections for $(\pi^- p)$, $(K^- p)$, and $(\bar{p}p)$ atom collisions with ordinary hydrogen. In Sec. IV the main results of the paper are summarized and possible effects of collision-induced absorption on the kinetics of the atomic cascade in hadronic atoms are briefly discussed.

Atomic units are used throughout the paper unless otherwise stated. The unit of cross sections is $a_0^2 = 2.8 \times 10^{-17}$ cm^2, where $a_0 = 5.29 \times 10^{-9}$ cm is the Bohr radius of the electron in the hydrogen atom.

II. CLOSE-COUPLING APPROACH

To give a fully quantum-mechanical treatment of collision-induced absorption in the scattering of hadronic hydrogen $(X^- p)$ from ordinary hydrogen, we apply the CCA developed in Refs. [11–18] to study exotic hydrogen–ordinary hydrogen collisions. Thus collision-induced absorption is described in a unified manner together with other collisional processes,

$$(X^- p)_{nl} + \mathrm{H} \to (X^- p)_{n'l'} + \mathrm{H}: \tag{6}$$

elastic scattering ($n' = n$, $l' = l$), Stark transitions ($n' = n$, $l' \neq l$), and Coulomb de-excitation ($n' \leqslant n - 1$).

A. Brief outline of the approach

The total wave function $\Psi(\boldsymbol{\rho},\mathbf{r},\mathbf{R})$ of the system $aX^- + be^-$ (a and b are nuclei of hadronic and ordinary atoms—in the present case, protons) satisfies the time-independent Schrödinger equation with the nonrelativistic Hamiltonian, which, after separating the center-of-mass motion, can be written as

$$H = -\frac{1}{2M_r}\Delta_{\mathbf{R}} + h_X(\boldsymbol{\rho}) + h_e(\mathbf{r}) + V(\mathbf{r},\boldsymbol{\rho},\mathbf{R}). \tag{7}$$

Here, M_r is the reduced mass of the system, and h_X and h_e are the Hamiltonians of the free hadronic and ordinary hydrogen atoms, respectively.

The interaction potential $V(\mathbf{r},\boldsymbol{\rho},\mathbf{R})$ includes the pair Coulomb interactions between the particles from two colliding subsystems and the strong interaction $\Delta V_{Xb}(\boldsymbol{\rho},\mathbf{R})$ between the hadron and the proton of the ordinary hydrogen atom as well.

The set of Jacobi coordinates $(\mathbf{R},\boldsymbol{\rho},\mathbf{r})$,

$$\mathbf{R} = \mathbf{R}_{e^-b} - \mathbf{R}_{X^-a}, \quad \boldsymbol{\rho} = \mathbf{r}_X - \mathbf{r}_a, \quad \mathbf{r} = \mathbf{r}_e - \mathbf{r}_b,$$

used in the present paper, is shown in Fig. 1. Here, $\mathbf{r}_a$, $\mathbf{r}_b$, $\mathbf{r}_X$, and $\mathbf{r}_e$ are the laboratory-system radius vectors of the nuclei, hadron, and electron; $\mathbf{R}_{e^-b}$, and $\mathbf{R}_{X^-a}$ are the center-of-mass radius vectors of the hydrogen and hadronic atoms, respectively.

The Hamiltonian of the hadronic atom is defined by

$$h_X = h_0 + \Delta V_{Xa}, \tag{8}$$

where h_0 is the Hamiltonian of the nonrelativistic Coulomb two-body problem having hydrogen-like eigenfunctions $|nlm\rangle$

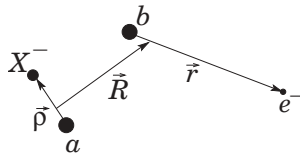

FIG. 1. Jacobi coordinates used to describe the (aX^-)–(be^-) collision.

and eigenvalues

$$E_n = -\frac{m_{Xa}}{2}\left(\frac{\alpha c}{n}\right)^2, \tag{9}$$

where m_{Xa} is the reduced mass of the hadronic atom, α the fine-structure constant, and c the velocity of light. The complex potential $\Delta V_{Xa}(\boldsymbol{\rho})$ is treated as a perturbation and takes into account all effects leading to the energy shift ΔE_{nl} from the Coulomb energy level E_n due to the vacuum polarization, the finite charge distribution, and, in the case of hadronic atoms, a strong interaction. In the leading order of perturbation theory one can obtain

$$\langle nlm|\Delta V_{Xa}(\boldsymbol{\rho})|nlm\rangle = \Delta E_{nl} = E_{nl}^{\mathrm{Re}} - i\Gamma_{nl}/2. \tag{10}$$

The real part E_{nl}^{Re} of the complex energy shift ΔE_{nl} is mainly determined by the strong interaction and electron vacuum polarization:

$$E_{nl}^{\mathrm{Re}} \cong \varepsilon_{nl}^{\mathrm{str}} + \varepsilon_{nl}^{\mathrm{vp}}. \tag{11}$$

The n dependence of ΔE_{ns} is described by the well-known formula

$$\Delta E_{ns} = \frac{\varepsilon_{1s}^{\mathrm{str}} - i\Gamma_{1s}/2}{n^3} + \varepsilon_{ns}^{\mathrm{vp}}, \tag{12}$$

while all sublevels with $l \geqslant 1$ are assumed to be the degenerated ones ($\Delta E_{nl} = 0$).

In a space-fixed coordinate frame the basis states $|1s,nl,L : JM\rangle$ are constructed from the ground-state wave function of an ordinary hydrogen, unperturbed hydrogen-like wave functions of a hadronic hydrogen in the $|n,l,m\rangle$ state, and the angular-momentum eigenfunctions $|L,\lambda\rangle$ of relative motion,

$$|1s,nl,L : JM\rangle = \frac{1}{\sqrt{4\pi}} R_{1s}(r) R_{nl}(\rho) \mathcal{Y}_{lL}^{JM}(\hat{\boldsymbol{\rho}},\hat{\mathbf{R}}), \tag{13}$$

where

$$\mathcal{Y}_{lL}^{JM}(\hat{\boldsymbol{\rho}},\hat{\mathbf{R}}) = \sum_{m\lambda} \langle lmL\lambda|JM\rangle Y_{lm}(\hat{\boldsymbol{\rho}}) Y_{L\lambda}(\hat{\mathbf{R}}). \tag{14}$$

In Eq. (14) the orbital angular momentum $\mathbf{l}$ of $(aX^-)_{nl}$ is coupled with the orbital angular momentum $\mathbf{L}$ of relative motion to give the total angular momentum $\mathbf{J} = \mathbf{l} + \mathbf{L}$. The exact wave function, corresponding to the real total energy E of the system, definite quantum numbers of the total angular momentum (J,M), and parity $\pi = (-1)^{l+L}$, and satisfying the Schrödinger equation

$$(E - H)\Psi_E^{JM\pi}(\mathbf{r},\boldsymbol{\rho},\mathbf{R}) = 0, \tag{15}$$

is expanded in terms of the basis states, Eqs. (13) and (14), as

$$\Psi_E^{JM\pi}(\mathbf{r},\boldsymbol{\rho},\mathbf{R}) = \frac{1}{R}\sum_{nlL} G_{nlL}^{EJ\pi}(R)|1s,nl,L : JM\rangle, \tag{16}$$

where $G_{nlL}^{EJ\pi}(R)$ are the radial functions of relative motion and the sum is restricted by the (l,L) values to satisfy the total parity conservation. This expansion leads to the multichannel scattering problem described by the coupled second-order differential equations for the radial functions $G_{nlL}^{EJ\pi}(R)$,

$$\left(\frac{d^2}{dR^2} + k_{nl}^2 - \frac{L(L+1)}{R^2}\right) G_{nlL}^{EJ\pi}(R) = 2M_r \sum_{n'l'L'} W_{nlL,n'l'L}^{J\pi}(R)\, G_{n'l'L'}^{EJ\pi}(R), \tag{17}$$

where

$$k_{nl}^2 = 2M_r E_{nl}^{\mathrm{ch}} \tag{18}$$

and

$$E_{nl}^{\mathrm{ch}} = E_{\mathrm{cm}} - \Delta_{nl,n_1l_1} \tag{19}$$

specify the channel wave number and energy, respectively, E_{cm} is the relative motion energy in the entrance (n_1l_1) channel, and, finally, Δ_{nl,n_1l_1} is the difference between the thresholds of the current and entrance channels,

$$\Delta_{nl,n_1l_1} = E_n + \Delta E_{nl} - E_{n_1} - \Delta E_{n_1l_1}. \tag{20}$$

The interaction-potential matrix $W_{n'l'L',nlL}^{J}$ coupling the asymptotic $(nlL;J)$ and $(n'l'L';J)$ channels is defined by

$$W_{n'l'L',nlL}^{J}(R) = \frac{1}{4\pi}\int d\mathbf{r}\, d\boldsymbol{\rho}\, d\hat{\mathbf{R}} R_{1s}^2(r) R_{nl}(\rho) R_{n'l'}(\rho) \times \mathcal{Y}_{lL}^{JM}(\hat{\boldsymbol{\rho}},\hat{\mathbf{R}})\, V(\mathbf{r},\boldsymbol{\rho},\mathbf{R}) \left[\mathcal{Y}_{l'L'}^{JM}(\hat{\boldsymbol{\rho}},\hat{\mathbf{R}})\right]^*. \tag{21}$$

These matrix elements are obtained by averaging the interaction potential $V(\mathbf{r},\boldsymbol{\rho},\mathbf{R})$ over the electron wave function $|1s\rangle$ and subsequently applying the addition theorem for spherical Bessel functions. The integration over $(\boldsymbol{\rho},\hat{\mathbf{R}})$ with the hadron hydrogen-like functions reduces the matrix element, Eq. (21), to the multiple *finite* sum (for details see [13]).

According to our study, the strong interaction potential $\Delta V_{Xb}(\boldsymbol{\rho},\mathbf{R})$ between the hadron and the proton of the target atom gives a negligibly small contribution to the interaction-potential matrix $W_{n'l'L',nlL}^{J}(R)$, Eq. (21), compared with both the Coulomb interactions and the complex energy shifts, Eq. (10), of the hadronic atom. Indeed, the interaction $\Delta V_{Xb}(\boldsymbol{\rho},\mathbf{R})$ may be described by an effective very short-range complex potential proportional to the δ function $\delta(\mathbf{R} - \xi\boldsymbol{\rho})$ ($\xi = m_a/(m_a + m_X)$). Then the corresponding additional coupling interaction is given by

$$\langle nlm|\Delta V_{Xb}(\boldsymbol{\rho},\mathbf{R})|nl'm'\rangle = \frac{\Delta E_{1s}}{|\phi_{1s}(0)|^2}\phi_{nlm}^*(\mathbf{R}')\phi_{nl'm'}(\mathbf{R}') \propto \frac{\Delta E_{1s}}{n^3}(R')^{l+l'}e^{-2R'}, \tag{22}$$

where $\phi_{nl'm'}(\mathbf{R}')$ is the hydrogen-like wave function of the hadronic atom, $\mathbf{R}' = m_X\mathbf{R}/n$. It is noteworthy that the energy shift due to the δ-like strong interaction is equal to 0 in the states of hadronic hydrogen with $l \neq 0$. This interaction leads to a very short-range coupling strongly suppressed at much lesser distances, $R \approx m_X^{-1} \sim 10^{-3}$ (m_X is the hadron mass in a.u.), than the main coupling $W_{n'l'L',nlL}^{J} \propto \exp(-2R)$ and gives a negligible contribution to the induced-absorption cross section[1] compared with the complex energy shift ΔE_{ns} in

[1]According to our study the additional effect of this coupling potential in the cross section of collision-induced absorption is about 10^{-4}% in the case of pionic hydrogen.

the hadronic atom. In the further consideration the effect of the strong interaction potential $\Delta V_{Xb}(\boldsymbol{\rho},\mathbf{R})$ is not taken into account.

Usually a channel is said to be open if $\mathrm{Re}E_{nl}^{\mathrm{ch}} > 0$ and closed if $\mathrm{Re}E_{nl}^{\mathrm{ch}} < 0$. The problem which we study in the present investigation is to describe hadronic hydrogen-ordinary hydrogen collisions in the framework of the CCA taking into account the states of hadronic hydrogen with finite lifetimes. Therefore, additional definition of the channels is necessary for the present study. Channels corresponding to quasidiscrete asymptotic states with $\mathrm{Im}E_{nl}^{\mathrm{ch}} > 0$ [due to the above-mentioned reactions, Eqs. (2)–(4)] are called unstable-state open channels if $\mathrm{Re}E_{nl}^{\mathrm{ch}} > 0$ and unstable-state closed ones if $\mathrm{Re}E_{nl}^{\mathrm{ch}} < 0$. In the present study we take into account both open and closed channels, some of which can be unstable-state channels. It must be emphasized that, in contrast to the division into open and closed channels, the boundary between stable- and unstable-state channels is washed out. Unstable states with negligible decay widths can be considered stable ones depending on the physical conditions, e.g., the collision energy.

In the present paper we are interested only in those solutions for which the entrance channel is open and stable, i.e., the total energy of the system is always real. The scattering S matrix is determined in the subspace of the open stable-state channels ($\mathrm{Re}E_{nl}^{\mathrm{ch}} > 0$ and $\mathrm{Im}k_{nl} = 0$) with the boundary conditions at $R \to \infty$ (incoming + outgoing waves) in terms of the spherical Ricatti-Bessel functions. In the case of both open and closed unstable-state channels the boundary conditions at $R \to \infty$ should be introduced in terms of the spherical Ricatti-Hankel functions $h_L^+(kR)$, which decrease exponentially at $R \to \infty$.

To determine the matrix elements of the S matrix one does not need to know the wave functions $G_{nlL}^{EJ\pi}(R)$ themselves. It is possible to determine the S matrix using only the ratios of these functions at the two nearest points R_m and $R_m + h$ in the asymptotic range (R_m is a matching point and h is an integration step):

$$D(R) = G(R)G^{-1}(R+h).$$

The main advantage of this approach is that the propagation matrix D is limited even for both closed and unstable-state channels in which the functions of the linearly independent solutions $G(R)$ can exponentially increase. Thus, the open and closed channels associated with both stable and unstable states are treated in a unified manner in the framework of this method. In all our calculations we used this propagation matrix method (for details see Appendix A in our recent paper [18]).

B. Cross sections

The partial-wave on-shell amplitude for the transition $i \to f$ [i and f are used to denote the initial (n,l,m) and final (n',l',m') quantum numbers of the hadronic atom states, respectively] is defined by the S^J matrix,

$$f_{i\to f}^J(\Omega) = \frac{i\sqrt{\pi}}{\sqrt{k_{nl}k_{n'l'}}} \sum_{LL'\lambda'} i^{L'-L}\sqrt{2L+1}\langle lmL0|Jm\rangle \times\left(\delta_{nlL,n'l'L'} - S_{nlL\to n'l'L'}^J\right)\langle l'm'L'\lambda'|Jm\rangle Y_{L'\lambda'}(\Omega), \quad (23)$$

where $\Omega = (\vartheta,\phi)$ is the center-of-mass scattering angle. The partial-wave differential and integral cross sections of the processes, (6), for the transitions $nl \to n'l'$, averaged over the initial distribution of the degenerated sublevels and summed over the degenerate final sublevels, are given by

$$\frac{d\sigma_{nl\to n'l'}^J}{d\Omega} = \frac{k_{n'l'}}{k_{nl}}\frac{1}{2l+1}\sum_{m,m'}\left|f_{nlm\to n'l'm'}^J(\Omega)\right|^2, \quad (24)$$

$$\sigma_{nl\to n'l'}^J = \frac{\pi}{k_{nl}^2}\frac{2J+1}{2l+1}\sum_{LL'}\left|\delta_{nlL,n'l'L'} - S_{nlL\to n'l'L'}^J\right|^2. \quad (25)$$

The total cross section is the sum of the partial ones:

$$\sigma_{nl\to n'l'} = \sum_J \sigma_{nl\to n'l'}^J. \quad (26)$$

In the case of hadronic atoms, the S matrix of the transitions is not unitary due to the instability of the low-angular-momentum states. The unitary defect allows one to determine the cross sections of collision-induced absorption or annihilation from nl states as follows:

$$\sigma_{nl}^{\mathrm{ind}} = \frac{\pi}{k_{nl}^2}\frac{1}{2l+1}\sum_J(2J+1) \times\sum_{LL'n'l'}\left(\delta_{nlL,n'l'L'} - \left|S_{nlL\to n'l'L'}^J\right|^2\right). \quad (27)$$

III. RESULTS

The CCA described in the previous section has been used to calculate the scattering cross sections for collisions of $\pi^- p$, $K^- p$, and $\bar{p}p$ atoms in excited states with hydrogen atoms. The present calculations had at least two purposes: first, to apply the fully quantum-mechanical approach to the study of collision-induced absorption in hadronic atoms and, second, to clear the effects of complex energy shifts of ns states of hadronic atoms on the cross sections of elastic scattering, Stark transitions, and Coulomb de-excitation.

Numerical calculations of the total cross sections of the processes, (6), and collision-induced absorption or annihilation have been performed for excited states of pionic, kaonic, and antiprotonic hydrogen with the principal quantum number $n_0 = 2$–8 and collision energies $E_{\mathrm{cm}} = 0.001$–100 eV. Calculations with physical values of complex energy shift have been performed using an extended basis set including all hadronic atom states with $n \leqslant n_0$. At all energies the convergence of the partial-wave expansion was achieved and all cross sections were calculated with an accuracy better than 0.1%.

The experimental values of the strong-interaction shifts and widths of the $1s$ state of pionic [19,20], kaonic [21], and antiprotonic [22] hydrogen used in the present paper are listed in Table I. The energy shift of the $1s$ state due to electron vacuum polarization for pionic [23], kaonic [21], and antiprotonic [22] hydrogen was also taken into account.

TABLE I. Values of the $1s$ energy-level shifts and widths.

Atom	$\pi^- p$	$K^- p$	$\bar{p}p$
$\varepsilon_{1s}^{\mathrm{str}}$ (eV)	-7.11 ± 0.3	283 ± 42	714 ± 14
$\varepsilon_{1s}^{\mathrm{vp}}$ (eV)	-3.24 ± 0.1	-19 ± 1	-43 ± 1
Γ_{1s} (eV)	0.76 ± 0.2	541 ± 111	1097 ± 42

The central values of the $1s$ energy-level shifts and widths were used as their physical values in the present calculations throughout the paper. For the ns state with $n \geqslant 2$ the energy shift due to electron vacuum polarization is approximately calculated according to $\varepsilon^{\rm vp}_{ns} = \varepsilon^{\rm vp}_{1s}/n^3$.

A. The main regularities of the absorption cross section

A large variety of the complex energy-shift values in hadronic atoms [see Table I and Eq. (12)] reveals some general regularities in the behavior of the induced-absorption cross section. Similar effects may also be observed in the scattering of other systems involving unstable states.

To illustrate these regularities the cross section $\sigma^{\rm ind}_{np}(E, \Gamma_{ns})$ has been calculated for the case of $(\pi^- p)_{2p} + {\rm H}_{1s}$ collision used here as a model example. At the fixed values of total angular momentum J and parity π we have a model with three coupled channels (nlL): $(2p, L = J - 1)$, $(2p, L' = J + 1)$, and the channel $(2s, L'' = J)$ associated with the unstable $2s$ state of pionic hydrogen. The channel $(2p, L = J)$ has the opposite parity and is not coupled with the others.

In Figs. 2 and 3 we show the Γ_{2s} dependence of the $\sigma^{\rm ind}_{2p}(E_{\rm lab}, \Gamma_{2s})$ calculated at $E_{\rm lab} = 10^{-6}$ eV for the different values of ${\rm Re}\Delta_{2s,2p}$. The values of ${\rm Re}\Delta_{2s,2p}$ are chosen in such a way that at a given energy $E_{\rm lab}$ the channel associated with the unstable $2s$ state was either closed (Fig. 2) or open (Fig. 3). The value of the collision energy is taken very small to demonstrate the effects of the complex energy shift explicitly.

As shown in Figs. 2 and 3, the behavior of the cross section of collision-induced absorption as a function of Γ_{2s} allows us to distinguish conventionally at least three regions with essentially different Γ dependences of the cross section. The first region corresponds to very small values of Γ_{2s} in comparison with the diagonal and nondiagonal interaction potentials as well as the *absolute* value of the real part of the channel energy $E^{\rm ch}_{2s} = E_{\rm cm} - \Delta_{2s,2p}$. In particular, the condition

$$\varkappa = \frac{\Gamma_{2s}}{2\left|{\rm Re}\, E^{\rm ch}_{2s}\right|} < 0.1 \tag{28}$$

is satisfied in the examples considered here.

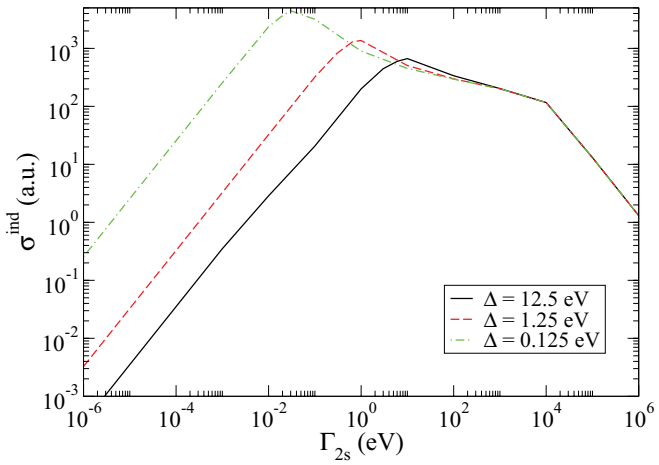

FIG. 2. (Color online) Cross section of collision-induced absorption for $(\pi^- p)_{2p} + {\rm H}$ scattering vs the width Γ_{2s} at a fixed value of laboratory kinetic energy $E_{\rm lab} = 10^{-6}$ eV and different values of $\Delta \equiv {\rm Re}\Delta_{2s,2p}$ corresponding to closed unstable-state channels.

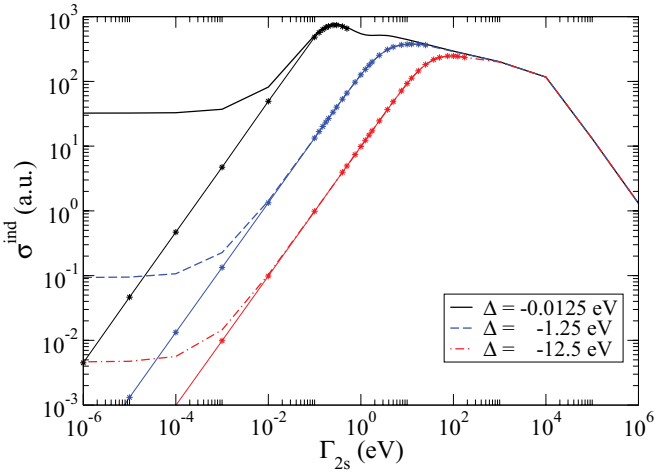

FIG. 3. (Color online) The same as Fig. 2 at different values of $\Delta \equiv {\rm Re}\ \Delta_{2s,2p}$ corresponding to an open unstable-state channel. The difference $[\sigma^{\rm ind}_{2p}(E, \Gamma_{2s}) - \sigma^{\rm ind}_{2p}(E,0)]$ is shown by the lines with asterisks.

In the case of closed unstable-state channels (Fig. 2) the cross section of collision-induced absorption increases in this region proportionally to Γ_{2s} and can be written as

$$\sigma^{\rm ind}_{2p}(E, \Gamma_{2s}) = \beta\Gamma_{2s}, \tag{29}$$

where β is a function of the collision energy $E_{\rm cm}$, Re $\Delta_{2s,2p}$, and some other parameters of the scattering problem.

Such behavior can be qualitatively explained within a simple model of potential scattering with the complex potential $V = V_1 - i\,V_2\,(V_2 > 0)$. The imaginary part V_2 is proportional to Γ_{2s} and can be considered a perturbation. The scattering matrix at a fixed total angular momentum can be written as $S = e^{2i\delta}$, where δ is the complex partial-wave phase shift $\delta = \delta_1 + i\delta_2$ ($\delta_2 > 0$ and $\delta_2 \simeq \eta\Gamma_{2s} \ll 1$). Then for the partial cross section of inelastic (induced absorption in our case) scattering we obtain

$$\sigma^{\rm ind} \propto 1 - |S|^2 = 1 - e^{-4\delta_2} = 4\delta_2 = 4\eta\Gamma_{2s}. \tag{30}$$

In the general case of the multichannel scattering problem, the unstable-state channel can be excluded from the system following Feshbach's method [24] (see also [25]). Then we obtain a complex addition to the interaction matrix $W_{\alpha\beta}$ between the "stable" channels:

$$\Delta W_{\alpha\beta} = W_{\alpha 0}(E_0 + i\Gamma_0/2 - T_0 - W_{00})^{-1} W_{0\beta}, \tag{31}$$

where α, β denote the channel indexes ($\alpha = \{n,l,L\}$) and index 0 corresponds to the unstable-state channel. This is an effective short-range (nonlocal and energy-dependent in general case) absorptive interaction due to the coupling of the "stable" channels with the unstable-state channel. When the unstable-state channel is closed ($E_0 < 0$), the imaginary part of this effective interaction is determined only by the imaginary part of the channel energy $\Gamma_0/2$ and is proportional to Γ_0 at small values of Γ_0:

$$ {\rm Im}\Delta W_{\alpha\beta} \propto \Gamma. $$

Thus, ${\rm Im}\Delta W_{\alpha\beta}$ can be regarded as a small perturbation. Further, in the eigenphase representation [26] the S matrix is

given by $\tilde{S}_{\alpha\beta} = \delta_{\alpha\beta} e^{2i\delta_\alpha}$, where δ_α is the complex eigenphase shift in channel α, $\delta_\alpha = \delta_\alpha^R + i\delta_\alpha^I$ ($\delta_\alpha^I > 0$). At small Γ the imaginary parts of the eigenphase shifts are proportional to Γ: $\delta_\alpha^I \approx \eta_\alpha \Gamma$. Then for the total cross section of induced absorption, we get an expression similar to Eq. (30):

$$\sigma^{\text{ind}} \propto \sum_\alpha \left(1 - \sum_\beta |\tilde{S}_{\alpha\beta}|^2\right) \approx 4 \sum_\alpha \delta_\alpha^I = 4\Gamma \sum_\alpha \eta_\alpha. \quad (32)$$

For an open unstable-state channel (Fig. 3), the cross section of collision-induced absorption in the first region depends linearly on Γ_{2s},

$$\sigma_{2p}^{\text{ind}}(E, \Gamma_{2s}) = \sigma_{2p}^{\text{ind}}(E,0) + \beta\Gamma_{2s}, \quad (33)$$

since at $\Gamma_{2s} \to 0$

$$\sigma_{2p}^{\text{ind}}(E,0) \equiv \sigma_{2p\to 2s}(E), \quad (34)$$

where $\sigma_{2p\to 2s}(E)$ is the cross section of the Stark $2p \to 2s$ transition. To demonstrate the similarity in the behavior of the cross sections σ^{ind} in the case of both closed and open unstable-state channels explicitly, the differences $[\sigma_{2p}^{\text{ind}}(E, \Gamma_{2s}) - \sigma_{2p}^{\text{ind}}(E,0)]$ are shown in Fig. 3 as well.

The cross section of induced absorption significantly decreases in the first region while $|\text{Re}\Delta_{2s,2p}|$ is increasing. This effect may be qualitatively explained by the weakening of the *effective coupling* $W_{npL',nsL}^J(R) G_{nsL}(R)$ between stable-state and unstable-state channels. Indeed, the asymptotic behavior of the radial function $G_{nsL}(R)$ of an unstable-state channel is given by

$$G(R) \propto \exp(ikR) = \exp(ik_{\text{re}}R)\exp(-k_{\text{im}}R), \quad (35)$$

where the real k_{re} and imaginary k_{im} parts of the wave number [under the condition, Eq. (28)] for the closed unstable-state channel is determined by

$$k_{\text{re}} \approx \frac{\Gamma_{2s}}{2}\sqrt{\frac{M_r}{2\left|\text{Re}\, E_{2s}^{\text{ch}}\right|}}, \quad (36)$$

$$k_{\text{im}} \approx \sqrt{2M_r \left|\text{Re}\, E_{2s}^{\text{ch}}\right|}. \quad (37)$$

The factor $\exp(-k_{\text{im}}R)$ in Eq. (35) essentially decreases the effective coupling between the stable- and unstable-state channels and leads to suppression of the induced-absorption cross section, while the *absolute* value of $\text{Re}\Delta_{2s,2p}$ is increasing.

In the case of an open unstable-state channel the real and imaginary parts of the wave number under the same condition, Eq. (28) (here, $\text{Re}\, E_{2s}^{\text{ch}} > 0$), are given by the expressions

$$k_{\text{re}} \approx \sqrt{2M_r\, \text{Re}E_{2s}^{\text{ch}}}, \quad (38)$$

$$k_{\text{im}} \approx \frac{\Gamma_{2s}}{2}\sqrt{\frac{M_r}{2\text{Re}\, E_{2s}^{\text{ch}}}}. \quad (39)$$

Here, collision-induced absorption also becomes less likely with increasing energy shift $\text{Re}\Delta\varepsilon_{2s,2p}$. However, in contrast to the previous case, the effective coupling becomes much weaker due to the *fast oscillations* of the radial function, Eq. (35), at large R.

Now we determine a qualitative condition under which an unstable-state channel can be treated as a stable one. Our estimation is based on Eqs. (35), (36), and (39). For an open unstable-state channel this condition can be written either as

$$\exp(-k_{\text{im}}R_0) \cong 1 \quad (40)$$

or in a form close to the classical condition, Eq. (1),

$$\frac{\Gamma_{ns}R_0}{2v_{ns}^{\text{ch}}} \ll 1, \quad (41)$$

where $v_{ns}^{\text{ch}} = \sqrt{2\text{Re}E_{ns}^{\text{ch}}/M_r}$ is the "*relative-motion velocity*" in the unstable-state channel and R_0 denotes the characteristic radius of interaction as in Eq. (1). At high-energy scattering ($E_{cm} \approx \text{Re}E_{ns}^{\text{ch}}$) both the classical, Eq. (1), and the quantum-mechanical, Eq. (41), conditions lead to similar estimations. At low-energy scattering E_{cm} may be much less than $\text{Re}E_{ns}^{\text{ch}}$ due to the large value of the real part E_{nl}^{Re} of the complex energy shift, and the classical condition is not justified.

In the case where the unstable-state channel is closed the classical condition, Eq. (1), makes no sense. Instead, the qualitative quantum-mechanical estimation can be obtained from Eqs. (35) and (36) similarly to the unstable-state open channel considered above:

$$\exp(ik_{\text{re}}R_0) \cong 1, \quad (42)$$

$$\frac{\Gamma_{ns}R_0}{2}\sqrt{\frac{M_r}{2|\text{Re}E_{ns}^{\text{ch}}|}} = \frac{\Gamma_{ns}R_0}{2\tilde{v}_{ns}^{\text{ch}}} \ll 1. \quad (43)$$

Here, $\tilde{v}_{ns}^{\text{ch}}$ has a dimension of velocity but has no physical meaning of the asymptotic channel velocity. It is noted that when the unstable-state channel is closed the induced-absorption cross section differs from 0 at all values of the width, even very small ones. Therefore, the qualitative condition allowing us to neglect the unstable-state width depends crucially on the physical problem under consideration and additional conditions are demanded. For example, the cross section of elastic scattering must be considered with an accuracy better than 1% or the unitarity defect cannot exceed 0.0001. It is noted that the conditions determined in Eqs. (40) and (42) do not take into account the dynamics of the scattering problem and can be considered only as a qualitative estimation of the unstable-state effects.

In the third region Γ_{2s} is much greater than all interaction potentials and the absolute value of the real part of the energy $|\text{Re}E_{2s}^{\text{ch}}|$ in the unstable-state channel. Here, the cross section of collision-induced absorption, in contrast to that in the first region, sharply decreases while Γ_{2s} is increasing and behaves as

$$\sigma_{2p}^{\text{ind}} \propto \frac{1}{\Gamma_{2s}}, \quad (44)$$

i.e., proportional to the lifetime of the unstable state. In Figs. 2 and 3 this region corresponds to $\Gamma_{2s} \gtrsim 10^4$ eV and the lifetime of the unstable state is much less in comparison with the collision time, i.e., the unstable state does not practically take part in the scattering. Indeed, the behavior of the radial wave function (outgoing wave) associated with the unstable-state channel at large distances is defined by Eq. (35) with $k_{\text{re}} = k_{\text{im}} \cong \sqrt{M_r\Gamma_{2s}/2}$. At $\Gamma_{2s} \gtrsim 10^4$ eV the condition $k_{\text{im}}R = k_{\text{re}}R \gg 1$ is already fulfilled at very small $R \lesssim 0.05$ a.u., which is much lower than the characteristic radii of

the interaction potentials. Therefore, the effective coupling between stable- and unstable-state channels becomes very "short-range" and can be neglected in the equations describing stable-state channels. Thus, the three-channel scattering problem, in the case considered here, is reduced to the two-channel one: $(2p, L = J - 1)$ and $(2p, L = J + 1)$. It is noted that a dependence on Γ_{2s} similar to Eq. (44) can also be obtained as in the case of small Γ_{2s} discussed above. Indeed, the effective interaction between stable channels obtained by exclusion of the unstable channel from the system of equations behaves at $\Gamma \to \infty$ as

$$\Delta W_{\alpha\beta} = W_{\alpha 0}(E_0 + i\Gamma_0/2 - T_0 - W_{00})^{-1} W_{0\beta} \to -\frac{2i}{\Gamma_0} W_{\alpha 0} W_{0\beta}. \quad (45)$$

This complex potential can be considered as a perturbation with a small parameter $1/\Gamma_0$. Therefore, the analysis applied in the case of small Γ_0 (the first region) can also be used for large Γ_0. We see that the unitarity defect and, therefore, the collision-induced absorption cross section are proportional to the small parameter $1/\Gamma_0$, i.e., the cross section behaves in accordance with Eq. (44) at very large Γ.

In the intermediate region of the width values $|\mathrm{Re}\, E_{2s}^{\mathrm{ch}}| \lesssim \Gamma_{2s} \lesssim 10^4$ eV the cross sections of collision-induced absorption very slowly decrease with an increase in Γ_{2s}. Indeed, the cross sections decrease by about an order of magnitude while Γ_{2s} increases by more than four orders of magnitude. Of note, this region in Fig. 2 corresponds to the physical values of the complex energy shifts of ns states in kaonic and antiprotonic hydrogen atoms.

The behavior of the elastic $2p \to 2p$ cross section is also correlated with the value of Γ_{2s}. The dependence of the elastic $2p \to 2p$ and induced-absorption (from the $2p$ state) cross sections on Γ_{2s} calculated at two values of the laboratory kinetic energy, $E_{\mathrm{lab}} = 0.05$ and 15 eV, with the physical value of $\mathrm{Re}\Delta_{2s,2p} = -1.26$ eV (the sum of the vacuum polarization and strong interaction shifts) is shown in Fig. 4. It is noted that in the case of pionic hydrogen channels associated with the unstable $2s$ state are always open.

At small values of $\Gamma_{2s} \leqslant 0.1$ eV the elastic cross sections change by about a few percent with an increase in Γ_{2s}. Using the above-mentioned model with the complex potential and considering Γ_{2s} as a perturbation, we obtain

$$\sigma_{\mathrm{el}} \propto 4(\eta\Gamma_{2s})^2 + 4(1 - 2\eta\Gamma_{2s}) \sin^2\delta_1 \simeq 4 \sin^2\delta_1. \quad (46)$$

While Γ_{2s} increases from its physical value, $\sim$0.1 eV, up to $\sim 10^3$ eV the elastic cross section sharply decreases (by about two orders of the magnitude) and reaches a value which can be calculated without the inclusion of the $2s$ state in the basis set. This suppression of the elastic cross section is a specific feature of scattering in the $n = 2$ state, since here the coupling between stable- and unstable-state channels is a unique origin of the dipole interaction. In contrast to the considered example, the increase in Γ_{ns} does not lead to a strong suppression of the elastic cross sections for scattering of the excited hadronic atoms with $n \geqslant 3$, since there is a dipole interaction between stable-state channels with different values of the internal angular momentum $l > 0$.

B. Induced absorption or Stark transition?

Here we return to the question about the stability or instability of hadronic atom states in the scattering problem. Strictly speaking, all states are unstable, but under some conditions of the scattering problem an unstable state can be approximately considered as a stable one (see the previous section). Correct interpretation of the scattering process is very important to describe the kinetics of the atomic cascade properly. Indeed, the results of the cascade calculations and corresponding predictions essentially depend, in particular, on the correct identification of the event of induced absorption or Stark transition. To clear up this question the dependence of the absorption cross sections on the kinetic energy of a pionic hydrogen atom in the $2p$ state is shown in Fig. 5. The calculations were performed at the physical value of the real

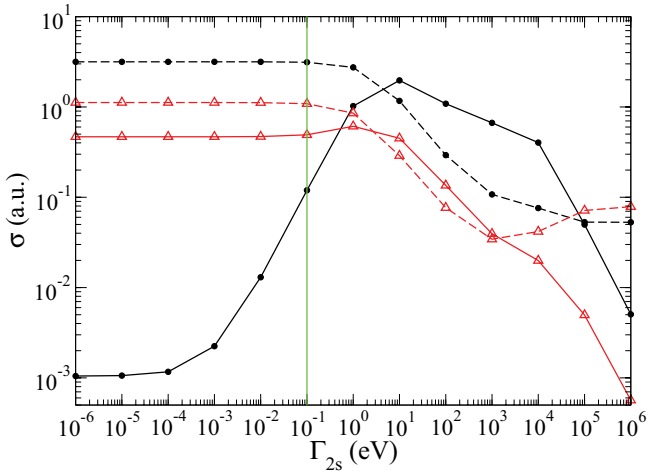

FIG. 4. (Color online) Elastic (dashed lines) and collision-induced absorption (solid lines) cross sections for $(\pi^- p)_{2p} + \mathrm{H}$ collisions vs the width Γ_{2s} at $E_{\mathrm{lab}} = 0.05$ (filled circles) and 15 eV (open triangles). The vertical line shows the physical value of $\Gamma_{2s} = 0.1$ eV.

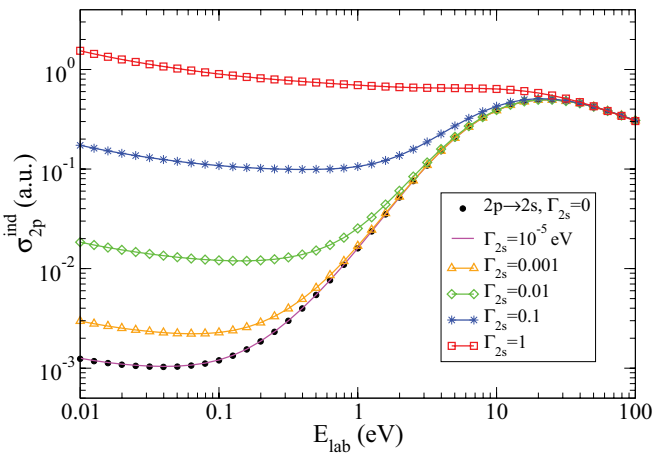

FIG. 5. (Color online) Induced-absorption cross sections for $(\pi^- p)_{2p} + \mathrm{H}$ collisions vs the laboratory kinetic energy E_{lab} calculated at different values of Γ_{2s}. The cross section of the Stark $2p \to 2s$ transition calculated at $\Gamma_{2s} = 0$ is shown for comparison (filled circles).

energy shift $\mathrm{Re}\Delta_{2s,2p} = -1.26$ eV and different values of Γ_{2s}, from 10^{-5} up to 1 eV. The energy dependence of the Stark mixing cross section calculated at $\Gamma_{2s} = 0$ is also presented in Fig. 5 for comparison. It is noted that at energies below 1 eV the Stark mixing cross section is strongly suppressed due to the large value of the real energy shift $\mathrm{Re}\Delta_{2s,2p} = -1.26$ eV.

At $\Gamma_{2s} = 10^{-5}$ eV, the induced absorption and Stark mixing ($\Gamma_{2s} = 0$) cross sections are indistinguishable (the relative difference does not exceed 1%) and the $2s$ state can be treated as a stable one since $\beta\Gamma_{2s} \ll \sigma_{2p}^{\mathrm{ind}}(E, \Gamma = 0)$ [see Eq. (33)]. The qualitative condition, Eqs. (40) and (41), is clearly satisfied and the pionic atom is more likely to be in the $2s$ state after the collision than to undergo induced absorption during the collision. Indeed, the imaginary part of the wave number k_{im} is determined here by Eq. (39) and the condition $k_{\mathrm{im}}R_0 \cong 2 \times 10^{-4} \ll 1$ is fulfilled at $R_0 \lesssim 5$ a.u. Then the exponentially decay factor in Eq. (35) satisfies the condition Eq. (40) with a high accuracy at all energies E_{cm} under consideration, i.e., the $\mathrm{Im}\Delta_{2s,2p}$ can be neglected and unstable-state channels can be treated as stable ones.

For width values $\Gamma_{2s} \geqslant 10^{-3}$ eV ($\Gamma_{2s} = 0.1$ eV corresponds to the physical value of the width), the absorption cross sections increase linearly with Γ_{2s} [see Eq. (33)] at a fixed energy and form a family of similar curves. It is worthwhile to note that for $\Gamma_{2s} \geqslant 10^{-3}$ eV the second term on the right-hand side of Eq. (33) becomes comparable to and even much larger than the first one and determines the value of the induced-absorption cross section in low-energy collisions. In this energy range $\mathrm{Re}E_{2s}^{\mathrm{ch}} \cong |\mathrm{Re}\Delta_{2s,2p}| = 1.26$ eV and the values of $k_{\mathrm{im}}R_0$ [see Eqs. (39) and (40)] are mainly determined by the value of Γ_{2s}. Here we obtain the values of the parameter $k_{\mathrm{im}}R_0 \gtrsim 10^{-2}$ at which the condition Eq. (35) is violated. According to our study, this condition is clearly fulfilled if $k_{\mathrm{im}}R_0 \lesssim (10^{-3}$–$10^{-4})$.

At a higher energy the condition $k_{\mathrm{im}}R_0 \cong 10^{-4} \ll 1$ is again fulfilled and the induced-absorption cross section approaches the cross section of the Stark $2p \to 2s$ transition at some energy E_{lab}^{*} correlated with the values of Γ_{2s} (e.g., for $\Gamma_{2s} = 10^{-3}$, 10^{-2}, and 10^{-1} eV the corresponding values of the energy $E_{\mathrm{lab}}^{*} \approx 3$, 10, and 33 eV, respectively). Such behavior of the absorption cross sections corresponds with the main regularities.[2]

According to our study, for energies $E_{\mathrm{lab}} \gtrsim 30$ eV (at the physical value of Γ_{2s}) the Stark transition $2p \to 2s$ is essentially more probable than induced absorption. Therefore, the pionic atom is destroyed due to charge-exchange reaction or radiative capture of the pion mainly after the Stark $2p \to 2s$ transition. In addition, we can conclude that the widths of the $n's$ sublevels formed in the process of the Coulomb transitions $nl \to n's$ ($n' \leqslant n - 1$) are always much less than the energies released in such transitions and the final $n's$ sublevels can be treated as stable ones.

The results obtained above allow us to conclude that in the general case one cannot simultaneously obtain the cross sections of collision-induced absorption and the Stark transition to the unstable state. Only under the definite conditions discussed above can an unstable state be approximately considered as a stable one.

In previous quantum-mechanical calculations [4] the effect of nuclear absorption during collisions was taken into account in the framework of a model in which the imaginary part of the ns-state energy shift was taken into account only for the interatomic separations $R \leqslant R_g = 5$ a.u. At $R > R_g$ the ns states of hadronic atoms in the model [4] were treated as normal asymptotic states and the imaginary part $(-\Gamma_{ns}/2)$ of the complex energy shift ΔE_{ns} was switched off independently of the value of the collisional energy and the conditions Eqs. (40) and (41). Moreover, the Stark transitions $nl \leftrightarrow ns$ together with the absorption during the collision and even the elastic scattering $ns \to ns$ have been considered in this model at all collision energies, although the lifetime of a hadronic atom in the ns state can be comparable to or even less than the characteristic time of the collision.

To illustrate the effect of the switched-off parameter R_g we present in Fig. 6 the energy dependence of the cross sections defined in [4]: absorption $\sigma_{2p\to\mathrm{abs}}$ and Stark transition $\sigma_{2p\to2s}$. The calculations were done using the model [4] with different values of the switched-off parameter, $R_g = 5$ and 15 a.u., for $(\pi p)_{n=2} + \mathrm{H}$ collisions. All cross sections were calculated in the framework of our numerical procedure. For comparison the cross sections of the Stark transition $\sigma_{2p\to2s}$ calculated for $\Gamma_{2s} = 0$ and $\sigma_{2p}^{\mathrm{ind}}$ calculated in the present approach with the correct boundary condition are also presented in Fig. 6. Both the absorption and, especially, the Stark cross sections, calculated in the framework of the model in [4], depend strongly on the value of R_g and cannot be treated reliably. At the same time the cross sections of the so-called maximum absorption $\sigma_{\max\,\mathrm{abs}} = \sigma_{2p\to\mathrm{abs}} + \sigma_{2p\to2s}$ calculated with $R_g \geqslant 5$ a.u. does not depend on the R_g value and practically coincides

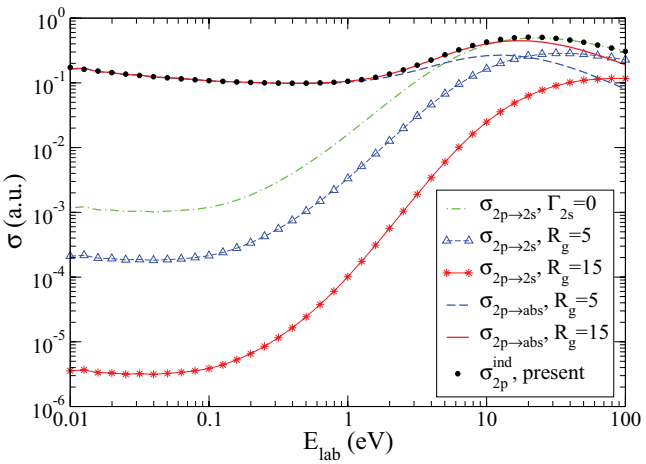

FIG. 6. (Color online) Cross sections of the absorption $\sigma_{2p\to\mathrm{abs}}$ and Stark transition $\sigma_{2p\to2s}$ (open triangles and asterisks) vs the laboratory kinetic energy calculated using the model in Ref. [4] for two values of the switched-off parameter $R_g = 5$ a.u. (dashed lines) and $R_g = 15$ a.u. (solid lines). The cross section of collision-induced absorption $\sigma_{2p}^{\mathrm{ind}}$ calculated in the present approach is denoted by filled circles. For comparison the Stark cross section $\sigma_{2p\to2s}$ calculated at $\Gamma_{2s} = 0$ is shown by the dash-dotted line.

[2]A similar observation was made in Ref. [6]: at energies much higher than the positronium level width (due to annihilation) the positron annihilation cross section approaches the cross section of positronium formation.

with the cross sections of the collision-induced absorption $\sigma^{\rm ind}$ calculated with the correct boundary conditions. In Fig. 6, the sections $\sigma_{\rm max\,abs}$ are not distinguishable from $\sigma_{2p}^{\rm ind}$ and therefore are not shown.

It is worthwhile noting that the results obtained in the framework of the close-coupling model [4] are more realistic than those obtained in the semiclassical approximation. However, for a reliable description of atomic cascade kinetics one must use a more elaborate approach for the proper description of all collision processes.

C. Pionic hydrogen

Numerical calculations have been done for the principal quantum number values and kinetic energies to provide comprehensive sets of the differential and total collisional cross sections needed for the detailed cascade calculations. Here we present a small portion of our results illustrating only the energy dependence of the total cross sections of collision-induced absorption calculated with the physical values of the ns-state energy shifts and widths. The results of the detailed calculations were used as input data in kinetics code and some results of the cascade calculations were recently published [26].

The energy dependence of the induced-absorption cross sections from the different sub-levels of pionic hydrogen in the states with $n = 6$ is shown in Fig. 7. At energies below ~0.1 eV the $\sigma_{nl}^{\rm ind}$ with various $l = 1, \ldots, 5$ have quite different energy behaviors. Such behavior is explained by the strong coupling of the different channels in the low-energy region.

At higher energies dipole coupling dominates and induced absorption from the np sublevels becomes more probable than from the states with $l > 1$. This statement is qualitatively supported by the simple estimation obtained in the dipole approximation, which is only justified in the high-energy region. Indeed, the l dependence of the interaction matrix elements coupling the sublevels at a fixed n can be obtained from Eq. (21) in the dipole approximation:

$$W^J_{nl\pm1,nl} \propto n\sqrt{n^2 - l^2}. \tag{47}$$

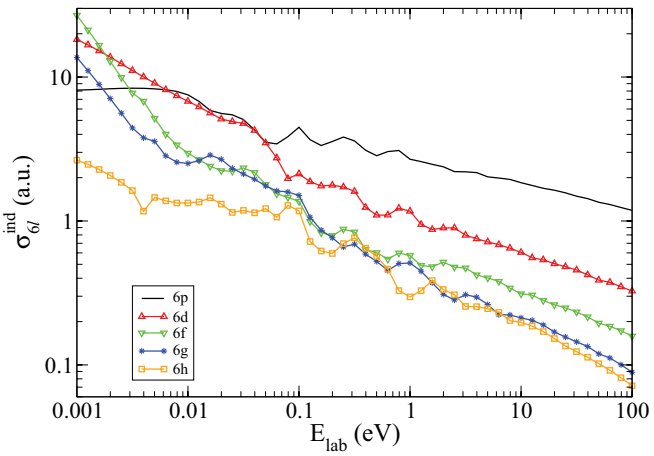

FIG. 7. (Color online) Energy dependence of the induced-absorption cross sections for $(\pi^- p)_{6l} + {\rm H}$ collisions.

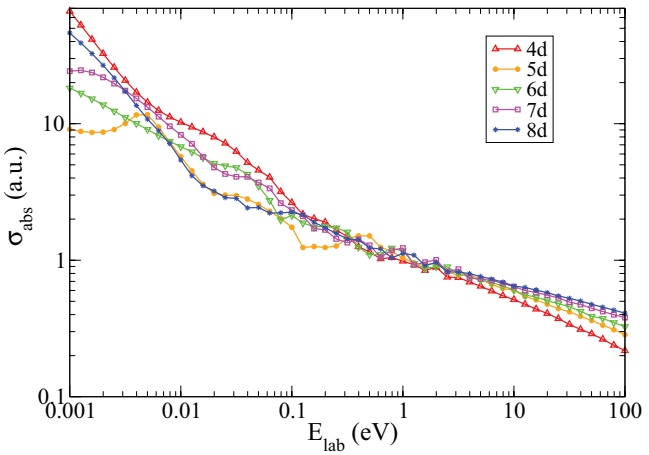

FIG. 8. (Color online) Energy dependence of the induced-absorption cross sections for $(\pi^- p)_{nd} + {\rm H}$ collisions.

Then the coupling matrix element, Eq. (47), e.g., for np states, is proportional to n^2, while for the circular orbit ($l = n - 1$) we obtain $W^J_{nn-2L\pm1,n\,n-1L} \propto n^{3/2}$. Also, additional suppression occurs due to the trivial statistical factor $1/(2l + 1)$ in Eq. (27). As a result, the differences between the induced-absorption cross sections from the $6p$ state and those from other states increase and reach about an order of magnitude at a collisional energy of more than a few electron volts. In accordance with our study in the previous section, at collisional energies $E_{\rm lab} > 10$ eV the induced-absorption cross sections from the $6l$ sublevels ($l \geqslant 1$) are practically equal to the cross sections of the Stark transitions calculated with $\Gamma_{6s} = 0$ (note that $\Gamma_{6s}/2 \approx 0.16 \times 10^{-3}$ eV) and can be treated as the cross sections of the Stark transitions.

Figure 8 shows the energy dependence of the induced-absorption cross sections calculated for the different nd states of pionic hydrogen with $n = 4$–8. In low-energy collisions the induced-absorption cross section as a whole grows while the n value decreases. This behavior corresponds qualitatively to the n dependence of the Γ_{ns}. At an $E_{\rm lab}$ of more than a few electron volts the n dependence of the coupling matrix elements becomes the most important and determines the behavior of the cross sections. As a result, we observe an increase in the cross section while n changes from 4 up to 8.

D. Kaonic hydrogen

The strong-interaction effects in the scattering of $K^- p$ atoms in excited states are rather different and can be essentially more important than in the case of pionic hydrogen. First, the real part ${\rm Re}\varepsilon_{1s}^{\rm str}$ of the $1s$ energy shift is repulsive and much larger in kaonic atoms, i.e., the binding energy of the ns states is lower than the binding energy of the $n\,l$ states with $l \geqslant 1$. Therefore, the unstable-state channels below the corresponding threshold energies $E_{\rm cm} < |{\rm Re}\Delta_{ns,nl}|$ are closed. Second, the strong-interaction width $\Gamma_{1s} = -2\,{\rm Im}\Delta E_{1s}$ in kaonic hydrogen is also much larger (by about two orders of magnitude) than in pionic hydrogen. It is important to note that for kaonic hydrogen the condition $|\Gamma_{ns}/2E_{ns}^{\rm Re}| \approx 1$ is always satisfied, in contrast to pionic hydrogen, for which the condition $|\Gamma_{ns}/2\Delta E_{ns}^{\rm Re}| \ll 1$ is fulfilled. Therefore, the widths

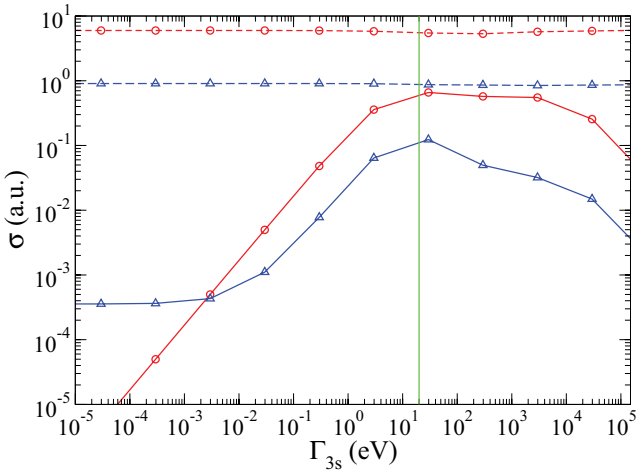

FIG. 9. (Color online) Elastic (dashed lines) and induced-absorption (solid lines) cross sections for $(K^- p)_{3p} + \mathrm{H}$ collisions vs the width Γ_{3s} calculated at $E_{\mathrm{lab}} = 1$ eV (open circles) and $E_{\mathrm{lab}} = 25$ eV (open triangles). The physical value of $\Gamma_{3s} = 20.04$ eV is shown by the vertical line.

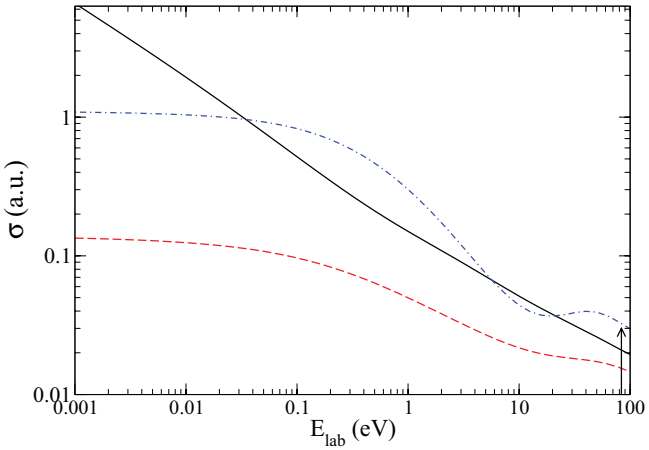

FIG. 10. (Color online) Energy dependence of the induced-absorption (solid line) and elastic scattering (dashed line) cross sections for $(K^- p)_{2p} + \mathrm{H}$ collisions. The elastic cross section calculated with $\Gamma_{2s} = 0$ is shown by the dash-dotted line. The $2s$ threshold energy is shown by the arrow.

Γ_{ns} cannot be considered as a perturbation in kaonic hydrogen scattering and must be taken into account within the realistic quantum-mechanical consideration. Finally, to our knowledge, the cross sections of collision-induced absorption for kaonic hydrogen and also all other collisional processes in the energy range below ns thresholds have not been calculated until now.[3]

The dependence of the elastic and induced-absorption cross sections for $(K^- p)_{3p} + \mathrm{H}$ collisions on the strong-interaction width Γ_{3s} is shown in Fig. 9. The calculations were performed in the wide range of values $\Gamma_{3s} = (10^{-5}$–$10^{5})$ eV and the two values of the laboratory kinetic energy $E_{\mathrm{lab}} = 1.0$ and 25 eV. Since the real part of the energy shift $\mathrm{Re}(\Delta_{3s,3p}) = 9.78$ eV, the unstable-state channels at $E_{\mathrm{lab}} = 1.0$ eV are closed, while at $E_{\mathrm{lab}} = 25$ eV they are open.

The main regularities of the induced-absorption cross section discussed in Sec. III A (see Figs. 2 and 3) are also revealed in the case of kaonic hydrogen. At a Γ_{3s} of less than a few electron volts, $\sigma_{3p}^{\mathrm{ind}}$ is proportional to Γ_{3s} when the unstable-state channels are closed and demonstrates a linear dependence on Γ_{3s} when the unstable-state channels are open. The numerical calculations confirm the validity of the conditions, Eqs. (40)–(43) in the case of kaonic hydrogen at nonphysical and very small values of Γ. In the intermediate region of Γ values these conditions are not satisfied and the unstable-state widths cannot be neglected. The physical value of $\Gamma_{3s} = 20.04$ eV is outside the region of linear dependence of the induced-absorption cross section on the width value. It is noted that the cross section calculated at $E_{\mathrm{lab}} = 25$ eV and the physical value of Γ_{3s} is about two orders of magnitude more than the cross section of the Stark transition $3p \to 3s$ calculated at $\Gamma_{3s} \to 0$. The cross section of elastic $3p$-$3p$ scattering is practically independent of Γ_{3s} since the $(3p$-$3d)$ coupling is stronger than the $(3p$-$3s)$-coupling due to the large value of the $(3p$-$3s)$ energy shift.

An example of the energy dependence of the collision-induced absorption and elastic cross sections for $(K^- p)_{2p} + \mathrm{H}$ scattering is shown in Fig. 10. The calculations were made with the physical value $\Gamma_{2s} = 67.6$ eV at collision energies both above and below the $2s$ threshold. At low energies the lowest partial waves make the main contribution to the cross sections of elastic scattering and collision-induced absorption. At energies of less than ~0.1 eV both the elastic scattering and the induced-absorption cross sections approach their threshold behavior: $\sigma_{2p}^{\mathrm{el}} \to \mathrm{const}$ and $\sigma_{2p}^{\mathrm{ind}} \propto 1/\sqrt{E}$.

Comparison of the elastic cross section calculated with the physical value of Γ_{2s} demonstrates strong suppression, of about an order of magnitude, compared with the cross section calculated at $\Gamma_{2s} = 0$. This suppression is explained by the much weaker effective coupling between the stable- and the unstable-state channels due to the fast oscillations of the wave function in the unstable-state channel. According to the present study the induced absorption from the $2p$ state of kaonic hydrogen is the fastest collision process at all energies under consideration and leads to suppression of the K_α yield at high target densities.

The energy dependencies of the calculated cross sections for the elastic $3p$-$3p$ scattering, Stark $3p \to 3d$ transition, Coulomb $3p \to 2p$ de-excitation, and induced absorption in $(K^- p)_{3p} + \mathrm{H}$ collisions are presented in Fig. 11. For energies higher than ~0.5 eV the elastic scattering and Stark $3p \to 3d$ transition are the fastest processes, while at lower energies the cross section of collision-induced absorption increases approximately as $\sigma_{2p}^{\mathrm{ind}} \propto 1/\sqrt{E}$ and becomes comparable to the cross sections of the elastic scattering and Stark mixing. In addition, the cross section of the Coulomb de-excitation $(3p \to 2p)$ is about an order of magnitude less than the cross sections of collision-induced absorption from both the $3p$ and the $3d$ states.

[3]The preliminary results for a kaonic hydrogen recently published in [10] were obtained using the experimental values of the strong-interaction shift and width of the $1s$ state from Ref. [27], which differ significantly from the data [21] used in the present calculations.

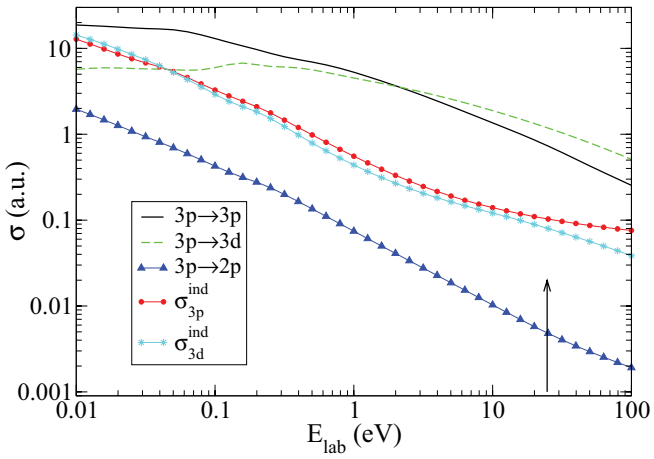

FIG. 11. (Color online) Energy dependence of the cross sections calculated for the elastic $3p$-$3p$ scattering, Stark $3p$-$3d$ transition, Coulomb $3p$-$2p$ de-excitation, and induced absorption in $(K^- p)_{3p}$ + H collisions. The arrow shows the $3s$ threshold energy.

Figure 12 shows the energy dependence of the induced-absorption cross sections for different sublevels of kaonic hydrogen with $n = 5$. At low collisional energies the induced-absorption cross sections from different sublevels ($5p$, $5d$, and $5g$) have comparable values and similar energy behavior due to the strong coupling of the different channels as well as in the case of pionic hydrogen scattering. At higher energies ($E_{\rm lab} \sim 2$–3 eV) the transitions with $|\Delta l| = 1$ dominate and induced absorption during collisions from the state with the lowest angular momentum (here the $5p$ state) becomes more probable than from the others.

Comparison of the present results with the results [4] of previous quantum-mechanical calculations (above the $5s$ threshold) and semiclassical calculations is also presented in Fig. 12. As a whole, there is satisfactory agreement of our induced-absorption cross sections with the so-called maximal absorption cross sections ($\sigma^{\rm abs}_{5p} + \sigma_{5p\to 5s}$) calculated in [4]. For energies below the $5s$ threshold the semiclassical approach [4] completely fails and cannot reproduce either the energy behavior or the absolute value of the induced-absorption cross sections.

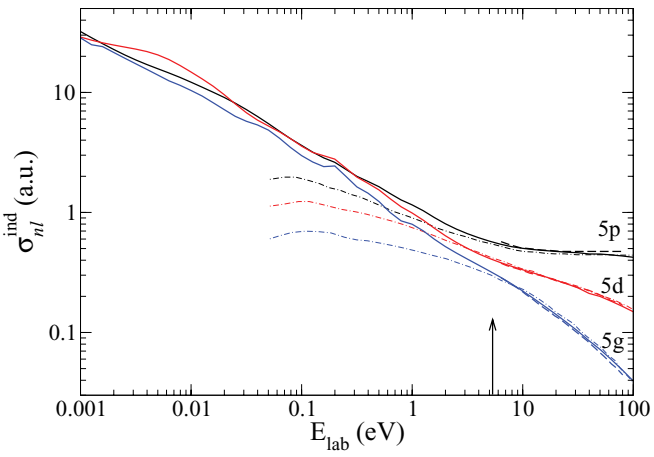

FIG. 12. (Color online) Induced-absorption cross sections for scattering of $K^- p$ in the $5p$, $5d$, and $5g$ states from hydrogen vs the laboratory kinetic energy. The present results are shown by solid lines; the results [4] of quantum-mechanical calculation, by the dashed line; and the results of semiclassical calculation, by the dash-dotted line. The arrow shows the $5s$ threshold energy.

E. Antiprotonic hydrogen

The effects of a strong interaction are enhanced in antiprotonic hydrogen in comparison with kaonic hydrogen. The values of the energy shifts and widths of the ns states in antiprotonic hydrogen are about two times larger than in $K^- p$. The real part of the ns energy shifts is also repulsive, therefore $nl \to ns$ transitions are forbidden below the corresponding threshold even at $\Gamma_{ns} = 0$. Another difference between kaonic and antiprotonic hydrogen is the hadronic width of the $2p$ state in antiprotonic hydrogen, $\Gamma_{2p} = 38 \pm 2.8$ meV [22], which is about two orders of magnitude larger than the radiative width, $\Gamma^{\rm rad}_{2p\to 1s} \cong 0.38$ meV, and must be taken into account in the realistic cascade model and in the quantum-mechanical calculations of low-energy collisions. According to our study, the $2p$ state of antiprotonic hydrogen can be treated as a normal asymptotic state for collision energies above $\sim$ 5–10 eV. In the examples considered below the effect of Γ_{np} is neglected in comparison with the much stronger effect of the complex energy shift of the ns state.

It is important to note one more peculiarity of antiprotonic hydrogen: ordinary hydrogen collisions due to the equality of the proton and antiproton masses. The matrix elements, Eq. (21), coupling the asymptotic initial $(nlL; J)$ and final $(n'l'L'; J)$ channels are identically equal to 0 if the internal orbital angular momenta satisfy the condition $(-1)^l = (-1)^{l'}$. Therefore the dipole coupling becomes more important in antiprotonic hydrogen scattering than in the case of pionic and kaonic atoms.

The energy dependence of the elastic cross sections for $(\bar p p)_{nl}$ atoms in the $5p$, $5d$, and $5g$ states scattering from hydrogen is shown in Fig. 13. There the results of the calculations with the physical value of $\Gamma_{5s}/2 = 4.2$ eV are

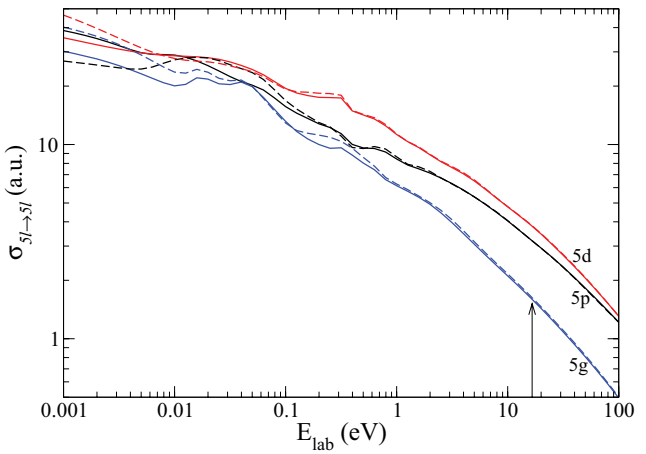

FIG. 13. (Color online) Energy dependence of the elastic cross sections for scattering of $\bar p p$ in the $5p$, $5d$, and $5g$ states from hydrogen. Results of the calculations with the physical value of $\Gamma_{5s}/2 = 4.2$ eV are shown by solid lines and those with $\Gamma_{5s} = 0$ by dashed lines. The arrow shows the $5s$ threshold energy.

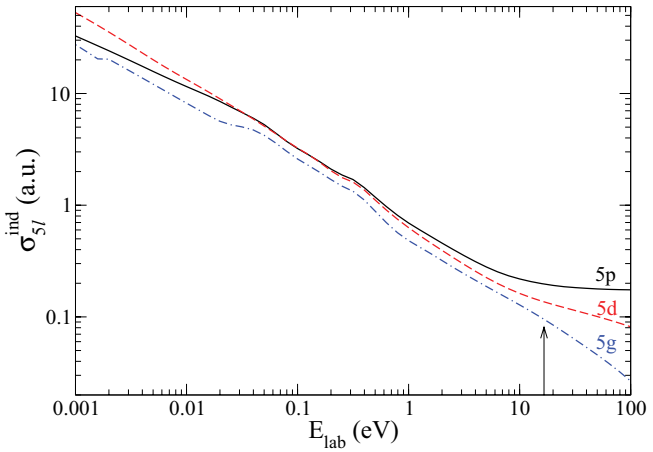

FIG. 14. (Color online) Cross sections of induced annihilation for scattering of $\bar{p}p$ in the $5p$, $5d$, and $5g$ states from hydrogen vs the laboratory kinetic energy ($\Gamma_{5s}/2 = 4.2$ eV). The arrow shows the $5s$ threshold energy.

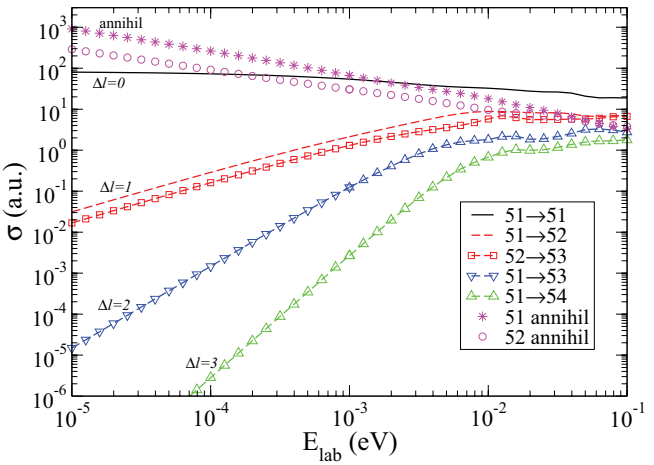

FIG. 16. (Color online) Threshold behavior of the elastic ($5l \to 5l$, $l \geqslant 1$), Stark ($5l \to 5l'$), and induced annihilation ($5l$, $l = 1$–2) cross sections for $\bar{p}p$ scattering from hydrogen ($\Delta l \equiv |l - l'|$).

compared with those obtained with $\Gamma_{5s} = 0$. Noticeable differences in the cross sections are only seen at low energies, $\lesssim$0.5 eV. At higher energies the influence of the width value becomes less pronounced. In accordance with the peculiarity discussed above, the cross section of elastic $5p$-$5p$ scattering is suppressed in comparison with the cross section of elastic $5d$-$5d$ scattering. The effect of a strong-interaction shift is enhanced for lower states and increases weakly for highly excited states of antiprotonic atoms.

Figure 14 shows an example of the energy dependence of induced-annihilation cross sections calculated for $5p$, $5d$, and $5g$ states of antiprotonic hydrogen. Both the energy and the l dependence of these cross sections are qualitatively very similar to the ones presented in Fig. 12 for kaonic hydrogen.

Figure 15 shows the energy dependence of the induced-annihilation cross sections for $(\bar{p})_{np}p$ collisions ($n = 3$–8). The energy behavior and n dependence of these cross sections

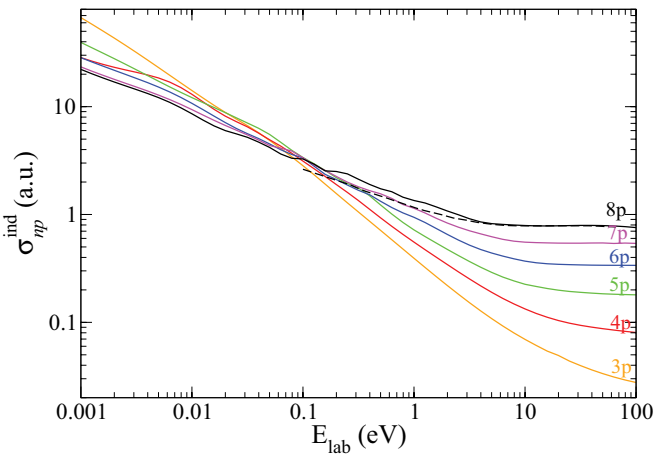

FIG. 15. (Color online) Cross sections of induced annihilation for $(\bar{p}p)_{np}$ ($n = 3$–8) scattering from hydrogen vs the laboratory kinetic energy. The present results are shown by solid lines; the results of semiclassical calculation (for the $8p$ state) from [4], by dashed lines.

are, as a whole, similar to the case of pionic hydrogen discussed above (see Fig. 8). Both of them grow while n is increasing. However, in contrast to pionic hydrogen, in the case of antiprotonic hydrogen we observe strong suppression of the induced-annihilation cross section from low-lying states due to the large values of the level shift and width. Comparison of the present results with the results of semiclassical calculations in [4] shows a satisfactory agreement for energies above ~4 eV. For lower energies the results of the semiclassical calculations underestimate the induced-annihilation cross sections (see also [10]) as in the case of kaonic hydrogen (see Fig. 12).

For proper description of the kinetics of the atomic cascade in hadronic atoms, knowledge of the low-energy behavior of the cross sections for different processes is very important. The threshold behavior of the elastic ($5l \to 5l, l \geqslant 1$), Stark ($5l \to 5l'$), and induced-annihilation ($5l$, $l = 1$–4) cross sections for $\bar{p}p$ scattering from hydrogen is illustrated in Fig. 16. It is shown that the threshold behavior of the cross sections begins at various energies below $E_{lab} \lesssim (3$–6×10^{-3} eV and, in correspondence with Wigner's law [28], is determined by simple energy dependencies: for induced annihilation $\sigma^{ind}(E_{lab}) \sim E_{lab}^{-1/2}$, and for the other processes $\sigma_{ll'}(E_{lab}) \sim E_{lab}^{|l-l'|}$ (l and l' are the orbital angular momenta of antiprotonic hydrogen in the initial and final states). It is noted that $|l - l'| \equiv \min(L + L')$, where L and L' are the orbital angular momenta of the relative motion.

IV. CONCLUSION

The fully quantum-mechanical description of induced absorption in $\pi^- p$ and $K^- p$ and induced annihilation in $\bar{p}p$ atoms has been studied in the framework of the CCA. The effects of complex energy shifts due to strong interaction and vacuum polarization have been taken into account straightforwardly in the quantum-mechanical scattering problem. Unstable states corresponding to both open and closed channels have been included in the basis set and the system of coupled second-order differential equations has been solved

with the correct boundary conditions using the propagation matrix method developed by the authors earlier.

In the framework of the present approach the cross sections of collision-induced absorption (in $\pi^- p$ and $K^- p$ atoms) and annihilation (in $\bar{p}p$ atoms) have been calculated in a unified manner together with the cross sections of elastic scattering, Stark transitions, and Coulomb de-excitation. The calculations have been done for states of the hadronic atoms with principal quantum numbers $n = 2$–8 and kinetic energies $E_{\rm lab} = 0.001$–100 eV.

The main regularities of the induced-absorption cross sections have been studied in a wide range of shifts and widths. In particular, in the case of pionic hydrogen it was shown that there are three regions of width values in which the dependencies of the induced-absorption cross sections on width are quite different, e.g., this dependence is linear at small widths of the unstable states. For kaonic and antiprotonic hydrogen atoms the corresponding regularities have also been studied, taking into account the fact that the values of their ns level shifts (repulsive) and widths are comparable and much larger than in the case of pionic hydrogen. The cross sections of all processes for collisions of kaonic and antiprotonic atoms with an ordinary hydrogen atom at energies below (np-ns) thresholds, including induced absorption and annihilation, have not been calculated before.

The quantum-mechanical condition that the unstable state can be approximately treated as a stable one in the scattering problem has been formulated for the general case of both the open and closed unstable-state channels. It has been shown that both the classical condition and quantum-mechanical conditions leads to the similar estimations if $E_{cm} \approx \mathrm{Re}E_{nl}^{ch}$.

Comparison of the present cross sections with those calculated earlier [4] in the close-coupling and semiclassical models shows, as a whole, a fairly good agreement, provided the collision energy is above the (np-ns) thresholds, while at lower energies the semiclassical description is not justified, strongly underestimates the induced-absorption cross sections, and cannot reproduce its energy and l dependencies.

In the case of pionic hydrogen the effects of induced absorption can be explicitly seen in the spectra of neutrons formed from the charge-exchange reaction $\pi^- + p \to \pi^0 + n$. There are at least three variants, which lead to different contributions to the neutron time-of-flight spectra.

(1) Coulomb transition $nl \to n's$ ($n' \leqslant n - 1$) and absorption from the $n's$ state: These must lead to peaks at energies corresponding to the energies of the preceding Coulomb transitions.

(2) Coulomb transition $nl \to n'l'$ ($n' \leqslant n - 1$; $l \neq 0$, $l' \neq 0$), elastic scattering, Stark transition $n'l' \to n's$, and, again, absorption from the $n's$ state: Here, the energy of the neutron may be lower than the energy obtained by the pionic hydrogen from the preceding Coulomb transition.

(3) Induced absorption from nl states ($l \neq 0$): In this case the energies of the formed neutrons change in wider boundaries—practically from the average energy of the target up to the estimated value (see discussion of Fig. 6).

Some results of the present study have been used in detailed kinetics calculations of the atomic cascade in pionic hydrogen [29].

This study reveals knowledge about induced absorption and annihilation in hadronic atoms during collisions with ordinary hydrogen that is very important for the reliable description and analysis of the x-ray yields and kinetic energy distribution of hadronic atoms at the instant of absorption or radiative transition. The latter has crucial meaning in the analysis of precision experiments aimed at the determination of strong-interaction widths (e.g., Γ_{1s} in pionic hydrogen and deuterium, Γ_{2p} in kaonic and antiprotonic hydrogen) with a very high accuracy.

We hope that the obtained results will allow the elimination of some uncertainties inherent in previous cascade calculations, in which different, and not always self-consistent and justified, assumptions are used to treat the collision processes.

ACKNOWLEDGMENTS

We would like to thank D. Gotta and L. Simons for their steadfast interest in our studies and G. Korenman for many useful discussions. This work was supported by RFBR Grant No. 10-02-01096 and IB BMBF Grant No. RUS 11/A03.

[1] M. Leon and H. A. Bethe, Phys. Rev. **127**, 636 (1962).
[2] E. Borie and M. Leon, Phys. Rev. A **21**, 1460 (1980).
[3] T. P. Terada and R. S. Hayano, Phys. Rev. C **55**, 73 (1997).
[4] T. S. Jensen and V. E. Markushin, Eur. Phys. J. D **19**, 165 (2002).
[5] A. Igarashi, M. Kimura, and I. Shimamura, Phys. Rev. Lett. **89**, 123201 (2002).
[6] A. Igarashi, M. Kimura, I. Shimamura, and N. Toshima, Phys. Rev. A **68**, 042716 (2003).
[7] G. Korenman and S. Yudin, arXiv:0711.4048.
[8] G. Korenman and S. Yudin, J. Phys.: Conf. Ser. **88**, 012060 (2007).
[9] P. Fraser, K. Amos, L. Canton, G. Pisent, S. Karataglidis, J. P. Svenne, and D. van der Knijff, Phys. Rev. Lett. **101**, 242501 (2008).
[10] V. N. Pomerantsev and V. P. Popov, Hyperfine Interact. **209**, 69 (2012).
[11] G. Ya. Korenman, V. N. Pomerantsev, and V. P. Popov, JETP Lett. **81**, 543 (2005); arXiv:nucl-th/0501036.
[12] V. N. Pomerantsev and V. P. Popov, JETP Lett. **83**, 331 (2006).
[13] V. P. Popov and V. N. Pomerantsev, arXiv:0809.0742.
[14] V. N. Pomerantsev and V. P. Popov, Phys. Rev. A **73**, 040501(R) (2006).
[15] V. P. Popov and V. N. Pomerantsev, arXiv:nucl-th/0512107.
[16] V. P. Popov and V. N. Pomerantsev, arXiv:0712.3111.
[17] V. P. Popov and V. N. Pomerantsev, Hyperfine Interact. **138**, 109 (2001).
[18] V. P. Popov and V. N. Pomerantsev, Phys. Rev. A **83**, 032516 (2011).
[19] H.-Ch. Schröder *et al.*, Eur. Phys. J. C **21**, 473 (2001).
[20] A. Hirtl *et al.*, Hyperfine Interact. **193**, 153 (2008).
[21] M. Bazzi *et al.*, Phys. Lett. B **704**, 113 (2011).
[22] D. Gotta, Prog. Part. Nucl. Phys. **52**, 133 (2004).

[23] S. Jonsell, J. Wallenius, and P. Froelich, Phys. Rev. A **59**, 3440 (1999).
[24] H. Feshbach, Ann. Phys. **5**, 357 (1958).
[25] N. F. Mott and H. S. W. Massey, *The Theory of Atomic Collisions* (Clarendon Press, Oxford, 1965), Chap. 14.
[26] M. Danos and W. Greiner, Phys. Rev. **146**, 708 (1966).
[27] G. Beer, A. M. Bragadireanu, M. Cargnelli, C. Curceanu, J. P. Egger, H. Fuhrmann, C. Guaraldo, M. Iliescu, T. Ishiwatari, K. Itahashi, M. Iwasaki, P. Kienle, T. Koike, B. Lauss, V. Lucherini, L. Ludhova, J. Marton, F. Mulhauser, T. Ponta, L. A. Schaller, R. Seki, D. L. Sirghi, F. Sirghi, and J. Zmeskal (DEAR Collaboration), Phys. Rev. Lett. **94**, 212302 (2005).
[28] E. P. Wigner, Phys. Rev. **73**, 1002 (1948).
[29] V. P. Popov and V. N. Pomerantsev, Hyperfine Interact. **209**, 75 (2012).